This is the accepted manuscript made available via CHORUS. The article has been published as:

Nonequilibrium Andreev resonances in ballistic graphene Andreev interferometers

Asmaul Smitha Rashid, Le Yi, Takashi Taniguchi, Kenji Watanabe, Nitin Samarth, Régis Mélin, and Morteza Kayyalha

Phys. Rev. B **111**, L180504 — Published 7 May 2025

DOI: 10.1103/PhysRevB.111.L180504

Nonequilibrium Andreev resonances in ballistic graphene Andreev interferometers

Asmaul Smitha Rashid,[1,2] Le Yi,[3,2] Takashi Taniguchi,[4] Kenji Watanabe,[5] Nitin Samarth,[3,6,2] Régis Mélin,[7] and Morteza Kayyalha[1,2,*]

[1] *Department of Electrical Engineering, The Pennsylvania State University, University Park, Pennsylvania 16802, USA*
[2] *Materials Research Institute, The Pennsylvania State University, University Park, Pennsylvania 16802, USA*
[3] *Department of Physics, The Pennsylvania State University, University Park, Pennsylvania 16802, USA*
[4] *Research Center for Materials Nanoarchitectonics, National Institute for Materials Science, 1-1 Namiki, Tsukuba 305-0044, Japan*
[5] *Research Center for Electronic and Optical Materials, National Institute for Materials Science, 1-1 Namiki, Tsukuba 305-0044, Japan*
[6] *Department of Materials Science and Engineering, The Pennsylvania State University, University Park, Pennsylvania 16802, USA*
[7] *Université Grenoble-Alpes, CNRS, Grenoble INP, Institut NEEL, Grenoble, France*

(Dated: April 24, 2025)

We investigate the nonequilibrium populations of Andreev bound states (ABSs) in ballistic graphene three-terminal Josephson junctions (JJs). Our measurements reveal periodic resistance oscillations as a function of the superconducting phase, which is modulated by the applied magnetic flux. Additionally, we observe several voltage-induced crossovers, where resistance oscillations alternate between minima and maxima at integer flux quanta, corresponding to 0 and π phase shifts, respectively. We utilize a microscopic model for long ballistic Andreev interferometers, accounting for both perturbative and non-perturbative scattering processes. This model attributes the $0-\pi$ crossovers to phase-sensitive Andreev reflections (ARs), which convert normal current into ABSs with nonequilibrium populations. Our combined theoretical and experimental approach suggests that unconventional energy-phase relations, such as π-shifted ABSs, can be created in multiterminal JJs without relying on complex Cooper quartet or Floquet physics.

In superconductor-normal-superconductor (SNS) Josephson junctions (JJs), Andreev reflection at N-S interfaces leads to the formation of Andreev bound states (ABSs) [1–4]. At equilibrium, these ABSs occupy the lowest energy states and are fundamental to the emergent properties of hybrid superconducting systems, such as spinful Andreev levels [5–10] and topological phases [11]. Introducing additional superconducting leads in multiterminal JJs adds extra phase degrees of freedom to the ABS spectrum [12, 13], thereby enabling the exploration of higher-dimensional topological phases [13–18], Andreev modes hybridization [6, 19–22], and Cooper quartets [23–25].

When JJs are driven out of equilibrium by an external perturbation, such as a voltage bias [26, 27] or microwave irradiation [28–32], the lowest-energy ABSs are excited to higher energy levels. In this scenario, the external perturbation often introduces a time-dependent superconducting phase, triggering a nonadiabatic transition that significantly impacts the population and dynamics of the ABSs. These nonequilibrium ABSs offer a unique platform to explore a range of phenomena, including nontrivial current-phase relations [6, 33] and the formation of Floquet-Andreev states [31, 34–36].

The nonequilibrium dynamics of ABSs have been theoretically investigated in various systems, including diffusive Andreev interferometers [37], one-dimensional long junctions [38], quantum dots [39], and two and multiterminal JJs (MTJJs) [17, 40]. We note that the last category of devices, MTJJs, have been extensively explored with a different focus [41–45], uncovering a variety of phenomena, including topological phases [13–18, 46], Cooper quartets [25, 47–51], hybridization of Andreev modes [19–22, 52], and nonreciprocal superconducting transport [53–57]. Experimental studies of nonequilibrium ABSs have largely centered on diffusive JJs, where voltage-induced shifts in the chemical potential broaden the quasiparticle distribution function, leading to the observation of anomalous supercurrents [27, 58–60]. However, nonequilibrium processes in diffusive JJs are often short-lived and are thus challenging to study in detail [61, 62]. In contrast, ballistic JJs are expected to exhibit ABSs with enhanced lifetime [63], offering a more robust platform for studying nonequilibrium processes in quantum transport. Recent experiments have explored the inverse AC Josephson effect [44] and Floquet-induced Cooper quartets [64] in ballistic graphene multiterminal JJs. Despite these recent advances, the underlying dynamics and population of the ABSs in ballistic junctions remain largely unexplored.

In this work, we gain insights into nonequilibrium Andreev processes by investigating the interplay between the Fermi surface, superconducting phases, and voltage biases in ballistic graphene three-terminal Andreev interferometers. We investigate two distinct configurations: an all superconducting interferometer (SSS) and a phased-biased two-terminal JJ with an additional normal contact (SSN). In both cases, we observe periodic oscillations of resistance (R) with respect to the supercon-

* Corresponding author: mzk463@psu.edu

ducting phase difference φ. Notably, in the all superconducting interferometer, we find *multiple* voltage-induced crossovers where the oscillations alternate between minima (0 phase) and maxima (π phase) at integer multiples of the magnetic flux quantum.

To interpret our results, we employ a model, accounting for both ABSs and the nonequilibrium Fermi surface of graphene [63]. Unlike a recent report attributing the observed $0-\pi$ crossovers to nonequilibrium Cooper quartets [64], this model instead ascribes these crossovers to a phase-sensitive Andreev reflection process (phase-AR). In this framework, phase-ARs generate ABSs with nonequilibrium populations due to the finite chemical potential in graphene. In contrast to prior studies in diffusive JJs with normal contacts [27, 58–60], in ballistic JJs, we theoretically find that ABSs have longer lifetimes and smaller linewidth broadening [61–63]. This enhanced lifetime is consistent with the observation of multiple $0-\pi$ crossovers in our experiments. Our combined theoretical and experimental approach shows that conductance spectroscopy in SSS interferometers directly probes the nonequilibrium population of Andreev levels. Furthermore, our findings reveal that the crossovers are a unique feature of voltage-biased multiterminal JJs without the need for relying on more exotic phenomena, such as Cooper quartets and Floquet ABSs.

We fabricate all superconducting (SSS) Andreev interferometers on hBN/graphene/hBN van der Waals heterostructures, which are edge-contacted by Ti (10 nm)/Al (80 nm) electrodes [65]. The graphene channel is typically around 1.2 μm long and 0.5 μm wide. Figure 1(a) shows a scanning electron microscope (SEM) image of a representative three-terminal Andreev interferometer. The left, right, and top terminals are denoted as S_L, S_R, and S_T, respectively. Furthermore, terminals S_R and S_T in this geometry are connected by a superconducting loop. This loop allows us to control the superconducting phase φ between S_R and S_T via an external magnetic flux as $\varphi = 2\pi\Phi/\Phi_0$, where Φ is the magnetic flux and $\Phi_0 = h/2e$ is the flux quantum. We apply current I_{dc} to S_L and measure voltage V_{LT} between S_L and S_T. As a result, the three-terminal Andreev interferometer (S_L, S_R, S_T) is at (V_{LT}, 0, 0) bias voltage configuration. We note that the Al tunneling probe in this device exhibits resistance on the order of tens of MΩ and hence does not play any role in the transport properties of our Andreev interferometer; see results for another device without any tunneling probe in the supporting information (SI; see also Refs. [66–71] therein). To reduce Joule heating, we perform all the measurements at 300 mK if not otherwise specified [72].

We select graphene as a material of choice for our experiments because it offers ballistic transport, supports transparent superconducting contacts, and allows gate-tunability of the superconducting coupling [73–75]. Signatures of ballistic transport including Fabry-Pérot oscillations of the critical current in a two-terminal JJ, and gate dependence of the characteristic energy in a SSS device are summarized in section V of the SI. Finally, we design T-shaped devices such that all terminals are equidistantly connected to the graphene channel [53] with the distance between each pair of terminals from the graphene center around 0.6 μm as depicted in Fig 1(a).

We first explore the critical current modulation as a function of the superconducting phase in SSS interferometers. Figures 1(b) and (c) show the color plot of the differential resistance R as a function of the magnetic field B and, respectively, the bias voltage V_{LT} and the bias current I_{dc} at gate voltage $V_g = 0\ V$. The dark blue region corresponds to supercurrent with $R = 0$. We observe modulations of the supercurrent as a function of the magnetic flux. The period of the modulations is approximately ΔB = 0.8 G which is consistent with ΔB = 0.827 G, corresponding to one flux quantum for the enclosed superconducting loop area of 25 μm^2. We further observe a series of dark-bright regions (indicated by arrows) appearing outside of the superconducting region. To better illustrate these regions, we plot line cuts of R versus Φ/Φ_0 (corresponding to the red arrow in Figs. 1(b) and (c)) at various V_{LT}'s in Fig. 1(d). For $|V_{LT}| < 35\mu$V, we observe minima in the resistance oscillations at multiples of the flux quantum with a periodicity of Φ_0. As we increase the bias voltage ($|V_{LT}|$), we observe frequency doubling at $V_{LT} \approx$ -35 μV, beyond which π-phase shifted oscillations with maxima at multiples of flux quantum are dominant. Thus, changing the bias voltage produces $0-\pi$ crossovers in R versus φ. In total, we observe four crossovers for bias voltages $V_{LT} < \Delta = 180$ μeV, where Δ is the superconducting gap of aluminum; see section VII of the SI for line cuts corresponding to purple, yellow, and black arrows in Figs. 1(b) and (c).

To understand the role of the superconducting terminal S_L, we fabricate an SSN Andreev interferometer, where a normal terminal N_L, fabricated with Cr (10nm)/Au (80nm), replaces S_L. Here, we also apply current I_N to N_L and measure voltage V_{LT} between N_L and S_T as shown in Fig. 2(a). We observe similar periodic oscillations of the resistance with the superconducting phase marked by a black arrow in Fig. 2(b). These maps are generated by sweeping I_{dc} at different B fields with step sizes of 1 nA and 0.05 G, respectively. Because of the large step size of B, the cuts from Fig. 2(a) have a poor resolution (see section XII of the SI). To improve the quality of the data, we separately measure the differential resistance R by sweeping the B field with a step size of 0.01 G at different values of I_{dc} near the crossover as shown in Fig. 2(b). We note that due to flux trapping in between measurements, the curves show a horizontal shift ($\approx$ 0.5 G) in Fig. 2(b). However, unlike the SSS junction, which shows multiple $0-\pi$ crossovers, we only observe a single crossover in the SSN device. We attribute this finding to the broadening of the distribution function and elastic scattering at the normal metal–graphene interface [27, 75], leading to shorter Andreev resonance lifetimes. The shorter lifetime is consistent with quasiparticle poisoning arising from parity-nonconserving scattering pro-

cesses occurring in the SSN device; see sections II and III of the SI for more details.

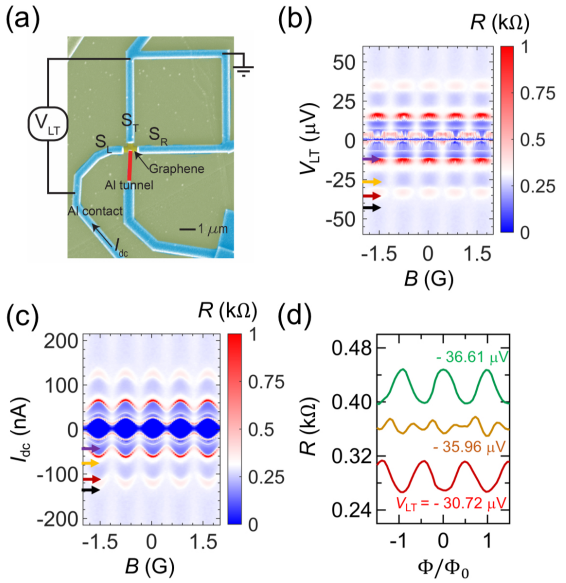


FIG. 1. (a) Scanning electron microscope (SEM) image of a representative three-terminal Andreev interferometer along with the measurement configuration. Current I_{dc} is applied to terminal S_L and voltage V_{LT} is measured between terminals S_L and S_T. The superconducting loop is grounded. (b, c) Differential resistance R as a function of the magnetic field B and V_{LT} (b) and bias current I_{dc} (c). Arrows mark $0-\pi$ crossovers. (d) Differential resistance R as a function of the magnetic flux Φ for the crossovers marked by the red arrows in (b) and (c). The oscillations show an evolution from minima to maxima with increasing $|V_{LT}|$. Curves are shifted vertically by 0.03 $k\Omega$ for clarity. Average value of V_{LT} is used in (d). Color maps are saturated to better highlight the $0-\pi$ crossovers. These maps are generated by sweeping B and I_{dc} with step sizes of 0.05 G and 1 nA, respectively.

We explore several potential mechanisms for $0-\pi$ crossovers in our experiment, including multiple Andreev reflections (MARs), normal current, self-induced Shapiro steps, and the phase-AR process. We note that the voltage range, where we observe the resonances, are very small ($\leq$ 50 μV), which if coming from MARs, would correspond to $n \geq 6$ (and even to $n \approx 27$), where $n = 2\Delta/eV_{LT}$ and $\Delta \approx 180$ μeV. Additionally, we do not find any resonance peak for n = 1, 2, 3, 4, and 5, further supporting our conclusion that MARs are likely not responsible for $0-\pi$ crossovers; see section VIII of the SI for more details.

To understand the impact of the normal current injection in graphene JJs, we fabricate two-terminal JJs with two additional normal contacts following Ref. [27]. Unlike Ref. [27], we observe that the critical current monotonically decreases with increasing normal current without any $0-\pi$ transition or supercurrent sign reversal; see section IX of the SI for more details.

Finally, we investigate the potential contribution of

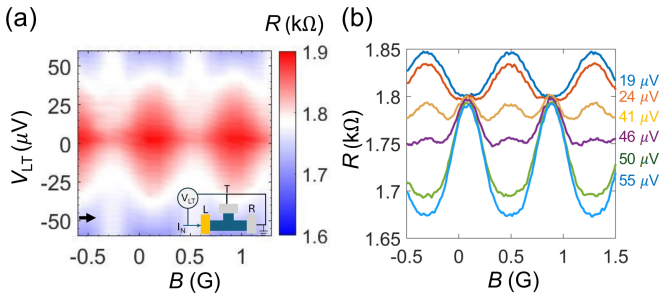


FIG. 2. (a) Differential resistance R as a function of the magnetic field B and V_{LT} for a three-terminal SSN device at a back gate voltage $V_g = 0$ V and temperature $T = 12$ mK. The Dirac point is at $V_{CNP} \approx$ -4.5 V. The inset shows the measurement setup. The superconducting terminals are denoted as S_T and S_R, and the normal terminal is denoted as N_L. Current I_N is applied to N_L and voltage V_{LT} is measurable between terminals N_L and S_T. (b) Differential resistance R versus B at different V_{LT}'s measured separately near the $0-\pi$ crossover. R is generated by sweeping B field with a step size of 0.01 G at different V_{LT}'s. The average value of V_{LT} is used in panel (b). The colormap is saturated to better highlight $0-\pi$ crossovers. Colormap is generated by sweeping B and I_{dc} with step sizes of 0.1 G and 1 nA, respectively.

self-induced Shapiro steps [76, 77] to the observed resonances by fabricating a two-terminal graphene JJ adjacent to the SSS interferometer. In the two-terminal JJ, we observe two self-induced Shapiro resonances for bias voltages within $\pm 25\mu$V ($|V_{bias}| \leq 25\mu$V). However, additional resonance peaks emerge in the SSS interferometer for $|V_{LT}| \geq 25\mu$; see section X of the SI for more details. Furthermore, in our SSN interferometer, where terminals S_R and S_T are grounded, Shapiro steps are entirely suppressed, consistent with our conclusion that self-induced Shapiro steps are likely not the source of the crossovers.

In the following, we describe the phase-AR process, which provides the most straightforward explanation for the observed resonance peaks and $0-\pi$ crossovers in both SSS and SSN interferometers. Figure 3(a) shows the schematics of the phase-AR process in a voltage-biased three-terminal Andreev interferometer. In two-terminal JJs, Cooper pair transfers are facilitated by low-energy ABSs with equilibrium populations, as both superconductors are at the same chemical potential. Likewise, in the SSS interferometer, when S_L is at zero bias voltage (V_{LT}= 0 V), Cooper pairs transmit between S_L and (S_R, S_T) via equilibrium ABSs. In contrast, a bias voltage applied to S_L changes the chemical potential of graphene. However, phase-dependent Cooper pair transfers still occur between terminals S_R and S_T, which remain grounded. This transfer process requires non-standard phase-sensitive ARs, giving rise to ABSs at higher energy levels. We have schematically represented this phase-AR process in Fig. 3(a), where the wavy line terminated by (ρ) denotes nonlocal coupling via the Keldysh Green's function in our model; see sections II

and III of the SI for more details.

Our theoretical model considers the device structure of Fig. 1(a) with superconducting phase variables $\varphi_R \simeq \varphi_0+\Phi/2$ and $\varphi_T \simeq \varphi_0-\Phi/2$, where φ_0 is the independent phase variable and Φ is the external magnetic flux threading the loop. In this case, the phase variable $\varphi_R-\varphi_T \simeq \Phi$ is the only static variable in our calculations, and other phase variables, e.g., $\varphi_{R,T}-\varphi_L$, have AC components when $V_{LT} \neq 0$. We note that our three-terminal Andreev interferometer operates in the AR regime for $V_{LT} \neq 0$, and the transport of Cooper pairs is primarily through AC Josephson oscillations of the current from S_L to S_R and S_T. The dissipative component of this current results in a change of the chemical potential by $\delta\mu_N = eV_{LT}$, which in turn leads to voltage-sensitive jumps in the nonequilibrium distribution function of graphene [63].

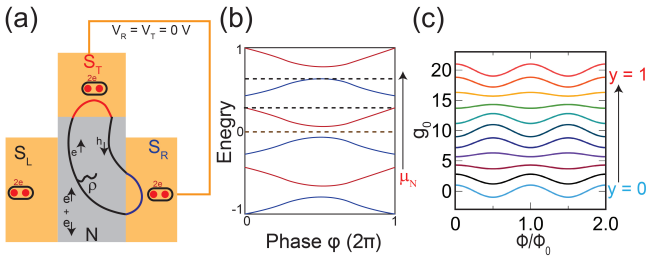


FIG. 3. (a) Schematics of the phase-Andreev refection (AR) process in a three-terminal Andreev interferometer where the wavy line represents coupling to the density of state in the normal region, via the nonlocal Keldysh Green's function. (b) The schematic diagram of energy versus phase relation of Andreev bound states (ABSs) with nonequilibrium populations. The dashed lines mark the chemical potential μ_N which changes with V_{LT}. (c) Theoretically calculated dimensionless conductance g_0 as a function of Φ/Φ_0 at various effective Fermi energies (y's).

Figure 3(b) schematically shows the spectrum of the nonequilibrium ABSs arising from the voltage-sensitive jumps in the chemical potential. These ABSs resemble those expected in the long-junction limit [2–4]. Our model predicts that the chemical potential μ_N (dash horizontal lines) increases with increasing V_{LT} and eventually crosses the spectrum at higher energy ABSs when $E(\varphi_T-\varphi_R) = \mu_N$. The high-energy ABSs exhibit π-shifted energy-phase relation, thereby resulting in the observation of π-shifted resonances in R versus φ. Alternating between different spectra of ABSs via further increase of μ_N will yield crossovers between resonances with maxima (minima) at multiples of flux quantum as shown by red (blue) curves. Experimentally, we observe that DC voltages (V_n's) corresponding to peaks in R are independent of V_g; see section V of the SI for more details. In long JJs, the energy level spacing of Andreev modes is proportional to the Fermi velocity v_F [2–4]. Therefore, v_F and, consequently, V_n's remain approximately constant with V_g due to the linear Dirac dispersion relation in graphene.

To calculate the differential conductance of the graphene Andreev interferometer, we assume an infinite planar geometry. We further assume the graphene interferometer is spatially uniform without any geometrical resonance. We calculate the current I_{LT} defined by Keldysh Green's functions and obtain the differential conductance dI_{LT}/dV_{LT} within the lowest-order perturbation theory as a function of bias voltage V_{LT} and current I_{LT}. We obtain a dimensionless differential conductance ($g_0 \propto dI_{LT}/dV_{LT}$) by taking the derivative of I_{LT} with respect to V_{LT}, where $g_0(\Phi/2\pi, V_{LT}R/\pi\hbar v_F) = \cos\Phi\cos(2eV_{LT}R/\hbar v_F)$. We note that unlike Ref. [64] where the quartet critical current ($I_q \propto \sin\varphi_q$) is responsible for crossovers, in our system, the conductance is proportional to $\cos\Phi$ instead of the expected $\sin\Phi$ for the equilibrium DC Josephson current between S_T and S_R. This $\cos\Phi$ term arises from phase-ARs, which are responsible for the conversion of normal current into supercurrent.

In ballistic devices, this model predicts that Andreev resonances are undamped and follow the $\cos(2eV_{LT}R/\hbar v_F)$, where $E = eV_{LT}$ is the bias voltage energy, $\tau = R/v_F$ is the ballistic propagation delay between S_R and S_T, and v_F is the Fermi velocity [63]. These undamped conductance oscillations are distinct from the damping predicted in the diffusive limit [37] and exhibit multiple sign changes and $0-\pi$ crossovers, consistent with our experiments; see section IV of the SI for more details. Figure 3(c) plots the calculated g_0 as a function of Φ/Φ_0 and effective Fermi energy $y = V_{LT}\ R/\pi\hbar v_F$. We observe multiple $0-\pi$ crossovers with increasing bias voltage V_{LT} in this theoretical plot, corroborating the experimental findings in Figs. 1 and 2. Our model predicts equally spaced resonances as shown in Fig. 3(c), which result from specific assumptions about linearized dispersion relations within a perfect waveguide geometry. However, replacing the rectangular graphene section with a chaotic cavity is expected to yield unequally spaced Andreev resonances [78], more closely resembling the experimental observations in Figs. 1 and 2. Finally, we find theoretically that the line width broadening of ABSs is reduced by a factor of η_s/Δ in SSS devices compared to SSN interferometers, where η_s is Dynes parameter. The emergence of a long timescale and small linewidth broadening points to the protection of the ABSs against the short relaxation time of the quasiparticle continua.

In conclusion, we used conductance spectroscopy to probe the nonequilibrium occupation of ABSs in voltage-biased three-terminal graphene JJs. We investigated three-terminal Andreev interferometers with superconducting contacts (SSS) and two-terminal JJs with normal contacts (SSN). In both cases, we observed periodic resonances in R versus φ, which we attributed to the energy-phase relation of nonequilibrium ABSs. In the SSS interferometer, we further observed several $0-\pi$ crossovers, where the resistance oscillations exhibit alternating 0 and π phase shifts with minima and maxima at integer flux quanta, respectively. Conversely, in the SSN interferome-

ter, the crossovers are suppressed and only one crossover is observed. To understand the microscopic mechanisms of these crossovers, we employed a model based on the phase-AR mechanism that converts normal current to supercurrent. This model predicts that Andreev resonances are undamped in ballistic JJs, resulting in multiple $0-\pi$ crossovers in the conductance, consistent with our experimental observations. We considered several possible mechanisms for the observed crossovers, including MARs and self-induced Shapiro steps, and concluded that the phase-AR process provides the simplest explanation for both SSN and SSS configurations. However, the comparison between our theoretical predictions and experimental data highlights the need for future investigations into inelastic scattering mechanisms and quasiparticle poisoning, employing more realistic modeling techniques. One promising direction for such future theoretical work is the adoption of density matrix calculations to provide a more accurate description. Future research may focus on direct measurements of the local density of states, e.g., through conductance and tunneling spectroscopy [79, 80], to elucidate the connection between phase-ARs and the theoretically predicted Floquet-Andreev states in multiterminal JJs.

The data supporting the conclusions of this letter is available on Zenodo [81].

ACKNOWLEDGMENTS

We acknowledge funding from the Pennsylvania State University Materials Research Science and Engineering Center supported by the US National Science Foundation (DMR 2011839). R.M. acknowledges support from the French CNRS in Grenoble and the German KIT in Karlsruhe, which is funded by the International Research Project SUPRADEVMAT. K.W. and T.T. acknowledge support from the JSPS KAKENHI (Grant Numbers 21H05233 and 23H02052) and World Premier International Research Center Initiative (WPI), MEXT, Japan.

[1] A. Furusaki and M. Tsukada, Current-carrying states in josephson junctions, Phys. Rev. B **43**, 10164 (1991).
[2] I. O. Kulik, Macroscopic quantization and the proximity effect in s-n-s junctions, Soviet Journal of Experimental and Theoretical Physics **30**, 944 (1969).
[3] C. Ishii, Josephson currents through junctions with normal metal barriers, Progress of Theoretical Physics **44**, 1525 (1970).
[4] P. F. Bagwell, Suppression of the josephson current through a narrow, mesoscopic, semiconductor channel by a single impurity, Phys. Rev. B **46**, 12573 (1992).
[5] A. Zazunov, V. S. Shumeiko, E. N. Bratus', J. Lantz, and G. Wendin, Andreev level qubit, Phys. Rev. Lett. **90**, 087003 (2003).
[6] N. M. Chtchelkatchev and Y. V. Nazarov, Andreev quantum dots for spin manipulation, Phys. Rev. Lett. **90**, 226806 (2003).
[7] C. Padurariu and Y. V. Nazarov, Theoretical proposal for superconducting spin qubits, Phys. Rev. B **81**, 144519 (2010).
[8] M. Hays, V. Fatemi, D. Bouman, J. Cerrillo, S. Diamond, K. Serniak, T. Connolly, P. Krogstrup, J. Nygård, A. L. Yeyati, A. Geresdi, and M. H. Devoret, Coherent manipulation of an andreev spin qubit, Science **373**, 430 (2021).
[9] M. Pita-Vidal, A. Bargerbos, R. Žitko, L. J. Splitthoff, L. Grünhaupt, J. J. Wesdorp, Y. Liu, L. P. Kouwenhoven, R. Aguado, B. van Heck, A. Kou, and C. K. Andersen, Direct manipulation of a superconducting spin qubit strongly coupled to a transmon qubit, Nature Physics **19**, 1110 (2023).
[10] E. C. Gingrich, B. M. Niedzielski, J. A. Glick, Y. Wang, D. L. Miller, R. Loloee, W. P. Pratt Jr, and N. O. Birge, Controllable 0–π josephson junctions containing a ferromagnetic spin valve, Nature Physics **12**, 564 (2016).
[11] X.-L. Qi and S.-C. Zhang, Topological insulators and superconductors, Rev. Mod. Phys. **83**, 1057 (2011).
[12] J. A. Sauls, Andreev bound states and their signatures, Philosophical Transactions of the Royal Society A: Mathematical, Physical and Engineering Sciences **376**, 20180140 (2018).
[13] E. V. Repin, Y. Chen, and Y. V. Nazarov, Topological properties of multiterminal superconducting nanostructures: Effect of a continuous spectrum, Phys. Rev. B **99**, 165414 (2019).
[14] R.-P. Riwar, M. Houzet, J. S. Meyer, and Y. V. Nazarov, Multi-terminal josephson junctions as topological matter, Nature Communications **7**, 11167 (2016).
[15] J. S. Meyer and M. Houzet, Nontrivial chern numbers in three-terminal josephson junctions, Phys. Rev. Lett. **119**, 136807 (2017).
[16] L. Peralta Gavensky, G. Usaj, and C. A. Balseiro, Topological phase diagram of a three-terminal josephson junction: From the conventional to the majorana regime, Phys. Rev. B **100**, 014514 (2019).
[17] V. Chandrasekhar, Probing the topological band structure of diffusive multiterminal Josephson junction devices with conductance measurements, Applied Physics Letters **121**, 222601 (2022).
[18] L. P. Gavensky, G. Usaj, and C. A. Balseiro, Multiterminal josephson junctions: A road to topological flux networks, Europhysics Letters **141**, 36001 (2023).
[19] M. Coraiola, D. Z. Haxell, D. Sabonis, H. Weisbrich, A. E. Svetogorov, M. Hinderling, S. C. ten Kate, E. Cheah, F. Krizek, R. Schott, W. Wegscheider, J. C. Cuevas, W. Belzig, and F. Nichele, Phase-engineering the andreev band structure of a three-terminal josephson junction, Nature Communications **14**, 6784 (2023).
[20] S. Matsuo, T. Imoto, T. Yokoyama, Y. Sato, T. Lindemann, S. Gronin, G. C. Gardner, S. Nakosai, Y. Tanaka, M. J. Manfra, and S. Tarucha, Phase-dependent andreev molecules and superconducting gap closing in coherently-coupled josephson junctions, Nature Communications **14**, 8271 (2023).

[21] S. Matsuo, T. Imoto, T. Yokoyama, Y. Sato, T. Lindemann, S. Gronin, G. C. Gardner, M. J. Manfra, and S. Tarucha, Phase engineering of anomalous josephson effect derived from andreev molecules, Science Advances **9**, eadj3698 (2023).

[22] J. Pillet, V. Benzoni, J. Griesmar, J.-L. Smirr, and C. O. Girit, Nonlocal josephson effect in andreev molecules, Nano Letters **19**, 7138 (2019).

[23] R. Mélin, R. Danneau, and C. B. Winkelmann, Proposal for detecting the π-shifted cooper quartet supercurrent, Phys. Rev. Res. **5**, 033124 (2023).

[24] R. Mélin and D. Feinberg, Quantum interferometer for quartets in superconducting three-terminal josephson junctions, Phys. Rev. B **107**, L161405 (2023).

[25] M. Gupta, V. Khade, C. Riggert, L. Shani, G. Menning, P. Lueb, J. Jung, R. Mélin, E. P. A. M. Bakkers, and V. S. Pribiag, Evidence for π-shifted cooper quartets and few-mode transport in pbte nanowire three-terminal josephson junctions (2024), arXiv:2312.17703 [cond-mat.mes-hall].

[26] R. Mélin, R. Danneau, K. Yang, J.-G. Caputo, and B. Douçot, Engineering the floquet spectrum of superconducting multiterminal quantum dots, Phys. Rev. B **100**, 035450 (2019).

[27] J. J. A. Baselmans, A. F. Morpurgo, B. J. van Wees, and T. M. Klapwijk, Reversing the direction of the supercurrent in a controllable josephson junction, Nature **397**, 43 (1999).

[28] D. J. van Woerkom, A. Proutski, B. van Heck, D. Bouman, J. I. Väyrynen, L. I. Glazman, P. Krogstrup, J. Nygård, L. P. Kouwenhoven, and A. Geresdi, Microwave spectroscopy of spinful andreev bound states in ballistic semiconductor josephson junctions, Nature Physics **13**, 876 (2017).

[29] M. S. Rudner and N. H. Lindner, Band structure engineering and non-equilibrium dynamics in floquet topological insulators, Nature Reviews Physics **2**, 229 (2020).

[30] R. Mélin, J.-G. Caputo, K. Yang, and B. Douçot, Simple floquet-wannier-stark-andreev viewpoint and emergence of low-energy scales in a voltage-biased three-terminal josephson junction, Phys. Rev. B **95**, 085415 (2017).

[31] S. Park, W. Lee, S. Jang, Y.-B. Choi, J. Park, W. Jung, K. Watanabe, T. Taniguchi, G. Y. Cho, and G.-H. Lee, Steady floquet–andreev states in graphene josephson junctions, Nature **603**, 421 (2022).

[32] D. Z. Haxell, M. Coraiola, D. Sabonis, M. Hinderling, S. C. ten Kate, E. Cheah, F. Krizek, R. Schott, W. Wegscheider, W. Belzig, J. C. Cuevas, and F. Nichele, Microwave-induced conductance replicas in hybrid josephson junctions without floquet—andreev states, Nature Communications **14**, 6798 (2023).

[33] T. E. Golikova, M. J. Wolf, D. Beckmann, I. E. Batov, I. V. Bobkova, A. M. Bobkov, and V. V. Ryazanov, Nonlocal supercurrent in mesoscopic multiterminal sns josephson junction in the low-temperature limit, Phys. Rev. B **89**, 104507 (2014).

[34] T. Oka and S. Kitamura, Floquet engineering of quantum materials, Annual Review of Condensed Matter Physics **10**, 387 (2019).

[35] D. T. Liu, J. Shabani, and A. Mitra, Floquet majorana zero and π modes in planar josephson junctions, Phys. Rev. B **99**, 094303 (2019).

[36] D. J. Carrad, L. Stampfer, D. Olsteins, C. E. N. Petersen, S. A. Khan, P. Krogstrup, and T. S. Jespersen, Photon-assisted tunneling of high-order multiple andreev reflections in epitaxial nanowire josephson junctions, Nano Letters **22**, 6262 (2022), pMID: 35862144.

[37] P. E. Dolgirev, M. S. Kalenkov, A. E. Tarkhov, and A. D. Zaikin, Phase-coherent electron transport in asymmetric crosslike andreev interferometers, Phys. Rev. B **100**, 054511 (2019).

[38] B. J. van Wees, K.-M. H. Lenssen, and C. J. P. M. Harmans, Transmission formalism for supercurrent flow in multiprobe superconductor-semiconductor-superconductor devices, Phys. Rev. B **44**, 470 (1991).

[39] R. Mélin and B. Douçot, Inversion in a four-terminal superconducting device on the quartet line. ii. quantum dot and floquet theory, Phys. Rev. B **102**, 245436 (2020).

[40] R. Mélin, Inversion in a four-terminal superconducting device on the quartet line. i. two-dimensional metal and the quartet beam splitter, Phys. Rev. B **102**, 245435 (2020).

[41] N. Pankratova, H. Lee, R. Kuzmin, K. Wickramasinghe, W. Mayer, J. Yuan, M. G. Vavilov, J. Shabani, and V. E. Manucharyan, Multiterminal josephson effect, Phys. Rev. X **10**, 031051 (2020).

[42] G. V. Graziano, J. S. Lee, M. Pendharkar, C. J. Palmstr, and V. S. Pribiag, Transport studies in a gate-tunable three-terminal josephson junction, Phys. Rev. B **101**, 054510 (2020).

[43] A. W. Draelos, M.-T. Wei, A. Seredinski, H. Li, Y. Mehta, K. Watanabe, T. Taniguchi, I. V. Borzenets, F. Amet, and G. Finkelstein, Supercurrent flow in multiterminal graphene josephson junctions, Nano Letters **19**, 1039 (2019).

[44] E. G. Arnault, T. F. Q. Larson, A. Seredinski, L. Zhao, S. Idris, A. McConnell, K. Watanabe, T. Taniguchi, I. Borzenets, F. Amet, and G. Finkelstein, Multiterminal inverse ac josephson effect, Nano Letters **21**, 9668 (2021), pMID: 34779633.

[45] F. J. Matute-Cañadas, L. Tosi, and A. L. Yeyati, Quantum circuits with multiterminal josephson-andreev junctions (2023), arXiv:2312.17305 [cond-mat.mes-hall].

[46] E. Strambini, S. D'Ambrosio, F. Vischi, F. Bergeret, Y. V. Nazarov, and F. Giazotto, The ω-squipt as a tool to phase-engineer josephson topological materials, Nature Nanotechnology **11**, 1055 (2016).

[47] A. H. Pfeffer, J. E. Duvauchelle, H. Courtois, R. Mélin, D. Feinberg, and F. Lefloch, Subgap structure in the conductance of a three-terminal josephson junction, Phys. Rev. B **90**, 075401 (2014).

[48] E. G. Arnault, S. Idris, A. McConnell, L. Zhao, T. F. Larson, K. Watanabe, T. Taniguchi, G. Finkelstein, and F. Amet, Dynamical stabilization of multiplet supercurrents in multiterminal josephson junctions, Nano Letters **22**, 7073 (2022), pMID: 35997531.

[49] G. V. Graziano, M. Gupta, M. Pendharkar, J. T. Dong, C. P. Dempsey, C. Palmstrøm, and V. S. Pribiag, Selective control of conductance modes in multiterminal josephson junctions, Nature Communications **13**, 10.1038/s41467-022-33682-2 (2022).

[50] F. Zhang, A. S. Rashid, M. T. Ahari, W. Zhang, K. M. Ananthanarayanan, R. Xiao, G. J. de Coster, M. J. Gilbert, N. Samarth, and M. Kayyalha, Andreev processes in mesoscopic multiterminal graphene josephson junctions, Phys. Rev. B **107**, L140503 (2023).

[51] Y. Cohen, Y. Ronen, J.-H. Kang, M. Heiblum, D. Feinberg, R. Mélin, and H. Shtrikman, Nonlocal supercurrent

of quartets in a three-terminal josephson junction, Proceedings of the National Academy of Sciences **115**, 6991 (2018).
[52] M. Coraiola, D. Z. Haxell, D. Sabonis, M. Hinderling, S. C. ten Kate, E. Cheah, F. Krizek, R. Schott, W. Wegscheider, and F. Nichele, Spin-degeneracy breaking and parity transitions in three-terminal josephson junctions (2023), arXiv:2307.06715 [cond-mat.mes-hall].
[53] M. Gupta, G. V. Graziano, M. Pendharkar, J. T. Dong, C. P. Dempsey, C. Palmstrøm, and V. S. Pribiag, Gate-tunable superconducting diode effect in a three-terminal josephson device, Nature Communications **14**, 3078 (2023).
[54] M. Coraiola, A. E. Svetogorov, D. Z. Haxell, D. Sabonis, M. Hinderling, S. C. ten Kate, E. Cheah, F. Krizek, R. Schott, W. Wegscheider, J. C. Cuevas, W. Belzig, and F. Nichele, Flux-tunable josephson diode effect in a hybrid four-terminal josephson junction, ACS Nano **18**, 9221 (2024), pMID: 38488287.
[55] J. Chiles, E. G. Arnault, C.-C. Chen, T. F. Q. Larson, L. Zhao, K. Watanabe, T. Taniguchi, F. Amet, and G. Finkelstein, Nonreciprocal supercurrents in a field-free graphene josephson triode, Nano Letters **23**, 5257 (2023), pMID: 37191404.
[56] F. Zhang, A. S. Rashid, M. Tanhayi Ahari, G. J. de Coster, T. Taniguchi, K. Watanabe, M. J. Gilbert, N. Samarth, and M. Kayyalha, Magnetic-field-free nonreciprocal transport in graphene multiterminal josephson junctions, Phys. Rev. Appl. **21**, 034011 (2024).
[57] S. Matsuo, T. Imoto, T. Yokoyama, Y. Sato, T. Lindemann, S. Gronin, G. C. Gardner, M. J. Manfra, and S. Tarucha, Josephson diode effect derived from short-range coherent coupling, Nature Physics **19**, 1636 (2023).
[58] M. S. Crosser, J. Huang, F. Pierre, P. Virtanen, H. T. T., F. K. Wilhelm, and N. O. Birge, Nonequilibrium transport in mesoscopic multi-terminal sns josephson junctions, Phys. Rev. B **77**, 014528 (2008).
[59] P. E. Dolgirev, M. S. Kalenkov, and A. D. Zaikin, Interplay between josephson and aharonov-bohm effects in andreev interferometers, Scientific Reports **9**, 1301 (2019).
[60] D. Margineda, J. S. Claydon, F. Qejvanaj, and C. Checkley, Observation of anomalous josephson effect in nonequilibrium andreev interferometers, Phys. Rev. B **107**, L100502 (2023).
[61] R. C. Dynes, V. Narayanamurti, and J. P. Garno, Direct measurement of quasiparticle-lifetime broadening in a strong-coupled superconductor, Phys. Rev. Lett. **41**, 1509 (1978).
[62] F. Jaworski, W. H. Parker, and S. B. Kaplan, Quasiparticle and phonon lifetimes in superconducting pb films, Phys. Rev. B **14**, 4209 (1976).
[63] R. Mélin, A. S. Rashid, and M. Kayyalha, Ballistic andreev interferometers, Phys. Rev. B **110**, 235419 (2024).
[64] K.-F. Huang, Y. Ronen, R. Mélin, D. Feinberg, K. Watanabe, T. Taniguchi, and P. Kim, Evidence for 4e charge of cooper quartets in a biased multi-terminal graphene-based josephson junction, Nature Communications **13**, 3032 (2022).
[65] L. Wang, I. Meric, P. Huang, Q. Gao, Y. Gao, H. Tran, T. Taniguchi, K. Watanabe, L. Campos, D. Muller, *et al.*, One-dimensional electrical contact to a two-dimensional material, Science **342**, 614 (2013).
[66] B. S. Jessen, L. Gammelgaard, M. R. Thomsen, D. M. A. Mackenzie, J. D. Thomsen, J. M. Caridad, E. Duegaard, K. Watanabe, T. Taniguchi, T. J. Booth, T. G. Pedersen, A.-P. Jauho, and P. Bøggild, Lithographic band structure engineering of graphene, Nature Nanotechnology **14**, 340 (2019).
[67] V. Kammarchedu, D. Butler, A. S. Rashid, A. Ebrahimi, and M. Kayyalha, Understanding disorder in monolayer graphene devices with gate-defined superlattices, Nanotechnology **35**, 495701 (2024).
[68] C. Caroli, R. Combescot, P. Nozieres, and D. Saint-James, Direct calculation of the tunneling current, Journal of Physics C: Solid State Physics **4**, 916 (1971).
[69] C. Caroli, R. Combescot, P. Nozieres, and D. Saint-James, A direct calculation of the tunnelling current: Iv. electron-phonon interaction effects, Journal of Physics C: Solid State Physics **5**, 21 (1972).
[70] J. C. Cuevas, A. Martín-Rodero, and A. L. Yeyati, Hamiltonian approach to the transport properties of superconducting quantum point contacts, Phys. Rev. B **54**, 7366 (1996).
[71] M. Popinciuc, V. E. Calado, X. L. Liu, A. R. Akhmerov, T. M. Klapwijk, and L. M. K. Vandersypen, Zero-bias conductance peak and josephson effect in graphene-nbtin junctions, Phys. Rev. B **85**, 205404 (2012).
[72] M. Tomi, M. R. Samatov, A. S. Vasenko, A. Laitinen, P. Hakonen, and D. S. Golubev, Joule heating effects in high-transparency josephson junctions, Phys. Rev. B **104**, 134513 (2021).
[73] I. V. Borzenets, F. Amet, C. T. Ke, A. W. Draelos, M. T. Wei, A. Seredinski, K. Watanabe, T. Taniguchi, Y. Bomze, M. Yamamoto, S. Tarucha, and G. Finkelstein, Ballistic graphene josephson junctions from the short to the long junction regimes, Phys. Rev. Lett. **117**, 237002 (2016).
[74] J. Knoch, Z. Chen, and J. Appenzeller, Properties of metal–graphene contacts, IEEE Transactions on Nanotechnology **11**, 513 (2012).
[75] P. Pandey, R. Danneau, and D. Beckmann, Ballistic graphene cooper pair splitter, Phys. Rev. Lett. **126**, 147701 (2021).
[76] T. M. Klapwijk and J. E. Sepers, M.and Mooij, Regimes in the behavior of superconducting microbridges, Journal of Low Temperature Physics **138**, 801 (1977).
[77] D. D. Coon and M. D. Fiske, Josephson ac and step structure in the supercurrent tunneling characteristic, Phys. Rev. **138**, A744 (1965).
[78] M. Vanević and W. Belzig, Full counting statistics of andreev scattering in an asymmetric chaotic cavity, Phys. Rev. B **72**, 134522 (2005).
[79] L. Bretheau, J. I.-J. Wang, R. Pisoni, K. Watanabe, T. Taniguchi, and P. Jarillo-Herrero, Tunnelling spectroscopy of andreev states in graphene, Nature Physics **13**, 756 (2017).
[80] J. I.-J. Wang, L. Bretheau, D. Rodan-Legrain, R. Pisoni, K. Watanabe, T. Taniguchi, and P. Jarillo-Herrero, Tunneling spectroscopy of graphene nanodevices coupled to large-gap superconductors, Phys. Rev. B **98**, 121411 (2018).
[81] Nonequilibrium Andreev resonances in ballistic graphene Andreev interferometers [Data set]. Zenodo. (2025).